Evidence for hydrodynamic evolution in proton-proton scattering at 900 GeV

K. Werner,[1] Iu. Karpenko,[1,2] T. Pierog,[3] M. Bleicher,[4] and K. Mikhailov[5]
[1]*SUBATECH, University of Nantes-N2P3/CNRS-EMN, Nantes, France*
[2]*Bogolyubov Institute for Theoretical Physics, Kiev 143 03680, Ukraine*
[3]*Forschungszentrum Karlsruhe, Institut fuer Kernphysik, Karlsruhe, Germany*
[4]*Frankfurt Institute for Advanced Studies (FIAS), Johann Wolfgang Goethe Universitaet, Frankfurt am Main, Germany*
[5]*Institute for Theoretical and Experimental Physics, Moscow 117218, Russia*
(Received 5 October 2010; published 28 April 2011)

In pp scattering at 900 GeV, large numbers of elementary scatterings will contribute significantly, and the corresponding high-multiplicity events will be of particular interest. Elementary scatterings are parton ladders, identified with color flux tubes. In high-multiplicity events, many of these flux tubes are produced in the same space region, creating high-energy densities. We argue that there are good reasons to employ the successful procedure used for heavy-ion collisions: Matter is assumed to thermalize quickly, such that the energy from the flux tubes can be taken as an initial condition for a hydrodynamic expansion. This scenario gets spectacular support from very recent results on Bose-Einstein correlations in pp scattering at 900 GeV at LHC.

DOI: 10.1103/PhysRevC.83.044915 PACS number(s): 25.75.−q, 25.40.Ve, 13.85.−t

I. INTRODUCTION

After one decade of BNL Relativistic Heavy Ion Collider (RHIC) experiments it seems to be certain that heavy-ion collisions at RHIC energies produce a new state of matter that expands as an almost ideal fluid [1–8], whereas proton-proton scattering is usually considered to be a reference system, theoretically well under control via perturbative techniques. Although at very high energy, hadrons experience multiple scatterings when they hit protons or neutrons, inclusive cross-section calculations becomes quite simple owing to the fact that different multiple scattering contributions cancel owing to destructive interference (Abramovskii-Gribov-Kancheli cancellations). The corresponding formulas are simple and can be expressed in terms of parton distributions functions, based on evolution equations.

However, in particular at CERN Large Hadron Collider (LHC) energies where we expect large numbers of scatterings to contribute significantly, it becomes interesting to study event classes corresponding to a large number of scatterings (in practice: high-multiplicity events). Here one needs partial cross sections, corresponding to a particular multiple scattering type (single, or double, or triple, etc.). Gribov-Regge theory provides a solution, in particular when energy sharing is properly taken into account, as in the EPOS approach.

High-multiplicity events are very interesting for the following reasons: In EPOS, for example, a single scattering amounts to the exchange of a complete parton ladder, including initial-state radiation. The whole object is identified as a pair of color flux tubes, which finally break into many pieces (hadrons). In high-multiplicity events, with many scatterings involved, we have many parton ladders participating, and therefore a large number of flux tubes sitting essentially on top of each other, as in heavy-ion scattering at RHIC. In the heavy-ion case, we simply compute the energy density corresponding to these flux tubes (from string theory), assume thermalization, and then perform a hydrodynamic expansion based on these initial conditions [8].

Because the energy densities reached in high-multiplicity proton-proton collisions are comparable to the ones achieved in gold-gold scattering at RHIC, we apply the same procedure. The usual argument against this approach is the small size of the pp system, but because we know by now that the size of the space fluctuations in an event-by-event treatment in AuAu scattering is of the order of 1–2 fm, and AuAu seems to be driven by hydrodynamic flow, there is no reason not to do so for high-multiplicity pp. One should not forget that there is actually a long history of hydrodynamical tratment of pp scattering (see Refs. [9–12]).

In this paper, we briefly review the flux-tube/hydro approach of Ref. [8], with special emphasis on pp scattering. After some elementary checks concerning particle distributions, we come to the main result of this paper: The hydrodynamic expansion modifies drastically the space-time behavior of the evolution, compared to basic picture where the flux tubes decay independently. This space-time structure can be clearly "seen" when investigating Bose-Einstein correlations, and the recently published results from ALICE confirm the "hydrodynamic scenario."

II. MULTIPLE SCATTERING

A. Parton evolution

An elementary scattering within the EPOS approach [8] is given by a so-called "parton ladder" (see Fig. 1), representing parton evolutions from the projectile and the target side toward the center (small x). The evolution is governed by an evolution equation, in the simplest case according to Dokshitzer-Gribov-Lipatov-Altarelli-Parisi (DGLAP). In the following we refer to these partons as "ladder partons," to be distinguished from "spectator partons." Such a parton ladder may be considered as a longitudinal color field or flux tube, conveniently treated as a relativistic string. The intermediate gluons are treated as kink singularities in the language of relativistic strings. This

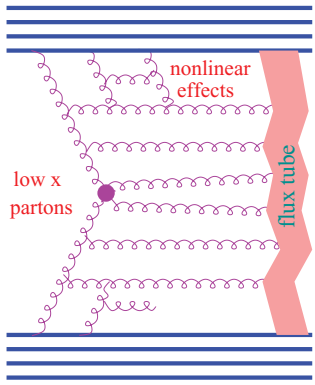

FIG. 1. (Color online) Elementary interaction in the EPOS model.

flux-tube approach is just a continuation of 30 years of very successful applications of the string picture to particle production in collisions of high-energy particles [13–16], in particular in connection with the parton model. An important issue at high energies is the appearance of so-called nonlinear effects, which means that the simple linear parton evolution is no longer valid, that gluon ladders may fuse or split. More recently, a classical treatment has been proposed, called color glass condensate (CGC), having the advantage that the framework can be derived from first principles [17–21]. Comparing a conventional string model such as EPOS and the CGC picture, they describe the same physics, although the technical implementation is, of course, different. All realistic string-model implementations have nowadays to deal with screening and saturation, and EPOS is not an exception (see Refs. [8,22]). Without screening, proton-proton cross sections and multiplicities will explode at high energies.

A phenomenological treatment of nonlinear effects in EPOS employs two contributions: a simple elastic rescattering of a ladder parton on a projectile or target nucleon (elastic ladder splitting) or an inelastic rescattering (inelastic ladder splitting) (see Fig. 2). The elastic process provides screening, therefore a reduction of total and inelastic cross sections. The importance of this effect should first increase with mass number (in case of nuclei being involved), but finally saturate.

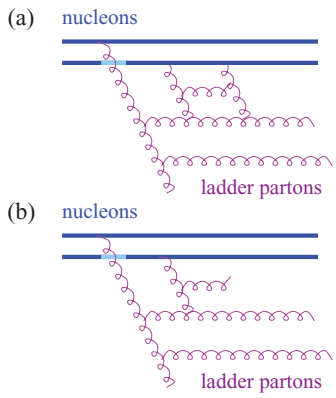

FIG. 2. (Color online) (a) Elastic "rescattering" of a ladder parton. We refer to elastic parton ladder splitting. (b) Inelastic "rescattering" of a ladder parton. We refer to inelastic parton ladder splitting.

The inelastic process will affect particle production. Both elastic and inelastic rescattering must be taken into account to obtain a realistic picture.

To include the effects of elastic rescattering, we first parametrize a parton ladder (to be more precise: the imaginary part of the corresponding amplitude in impact parameter space) computed on the basis of DGLAP. We obtain an excellent fit of the form $\alpha(x^+x^-)^\beta$, where x^+ and x^- are the momentum fractions of the "first" ladder partons on respectively projectile and target side (which initiate the parton evolutions). The parameters α and β depend on the cms energy $\sqrt{s}$ of the hadron-hadron collision. To mimic the reduction of the increase of the expressions $\alpha(x^+x^-)^\beta$ with energy, we simply replace them by

$$\alpha(x^+)^{\beta+\varepsilon_P}(x^-)^{\beta+\varepsilon_T}, \tag{1}$$

where the values of the positive numbers $\varepsilon_{P/T}$ will increase with the nuclear mass number and $\log s$.

The inelastic rescatterings (ladder splittings, looking from inside to outside) amount to providing several ladders close to the projectile (or target) side, which are close to each other in space. They cannot be considered as independent color fields (strings); we should rather think of a common color field built from several parton ladders. We treat this object via an enhancement of remnant excitations. In fact, the picture described so far is not yet complete, because we just considered two interacting partons, one from the projectile and one from the target. Also the remnants themselves contribute to particle production, but mainly in the fragmentation region. For more details, see Ref. [8].

B. Factorization and multiple scattering

An inclusive cross section is one of the simplest quantities to characterize particle production. As discussed earlier, inclusive cross section are particularly simple, quantum interference helps to provide simple formulas referred to a "factorization." If we want to study high-multiplicity events, we have to go beyond the inclusive treatment.

To formulate a consistent multiple scattering theory is difficult. A possible solution is Gribov's Pomeron calculus, which can be adapted to our language by taking "Pomeron" to mean "parton ladder." Multiple scattering means that one has contributions with several parton ladders in parallel. This formulation is equivalent to using the eikonal formula to obtain the total cross section from the knowledge of the inclusive one.

We indicated several years ago inconsistencies in this approach, proposing an "energy-conserving multiple scattering treatment" [15]. The main idea is simple: In case of multiple scattering, when it comes to calculating partial cross sections for double, triple, etc., scattering, one has to explicitly care about the fact that the total energy has to be shared among the individual elementary interactions. In other words, the partons ladders which happen to be parallel to each other share the collision energy (see Fig. 3). A consistent quantum mechanical formulation of these ideas requires not only the consideration of the usual (open) parton ladders, discussed so far, but also of closed ladders, representing elastic scattering.

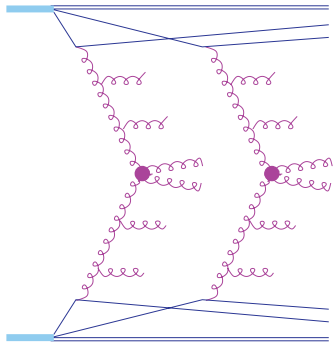

FIG. 3. (Color online) Multiple scattering with energy sharing.

These are the same closed ladders that we introduced earlier in connection with elastic rescatterings. The closed ladders do not contribute to particle production, but they are crucial because they affect substantially the calculations of partial cross sections. Actually, the closed ladders simply lead to large numbers of interfering contributions for the same final state, all of which have to be summed up to obtain the corresponding partial cross sections. It is a unique feature of our approach to consider explicitly energy-momentum sharing at this level (the "E" in the acronym EPOS). For more details, see Ref. [15].

III. HYDRODYNAMIC EVOLUTION

A. Parton ladders, flux tubes, energy-momentum tensor

In case of high-multiplicity pp scattering, we apply exactly the same procedure as we did for AuAu collisions at RHIC, as explained in detail in Ref. [8], and shortly reviewed in the following. We identify parton ladders with elementary flux tubes, the latter ones treated as classical strings. We use the simplest possible string: a two-dimensional surface $X(\alpha, \beta)$ in $3 + 1$-dimensional space-time, with piecewise constant initial conditions, referred to as kinky strings. In Fig. 4(a), we sketch the space components of this object: The string in $\mathbb{R}^3$ space is a mainly longitudinal object (here parallel to the z axis) but owing to the kinks (associated to transversely moving gluons) there are string pieces moving transversely (in the y direction in the picture). However, despite these kinks, most of the string carries only little transverse momentum.

In case of elementary reactions such as electron-positron annihilation or proton-proton scattering (at moderately relativistic energies), hadron production is realized via string breaking, such that string fragments are identified with hadrons. When it comes to heavy-ion collisions or very high energy proton-proton scattering, the procedure has to be modified, because the density of strings will be so high that they cannot possibly decay independently. For technical reasons, we split each string into a sequence of string segments, at a given proper time τ_0, corresponding to widths $\delta\alpha$ and $\delta\beta$ in the string parameter space [see Fig. 4(b)]. One distinguishes between string segments in dense areas (more than some critical density ρ_0 of segments per unit volume) from those in low-density areas. The high-density areas are referred to as core; the low-density areas are referred to as corona [23]. To

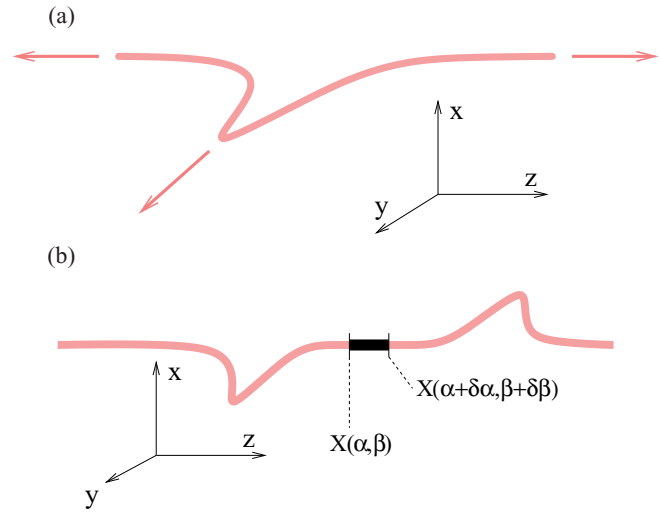

FIG. 4. (Color online) (a) Flux tube with transverse kink in $\mathbb{R}^3$ space. The kink leads to transversely moving string regions (transverse arrow). (b) String segment at given proper time.

compute densities, we employ a grid in hyperbolic coordinates x, y, η, τ, which correspond to the local comoving frame in case Bjorken hydrodynamics. In our case, the string dynamics leads to to a situation very close to the Bjorken case, in the sense that the average rapidity is equal to the space-time rapidity. String segments with large transverse momentum (close to a kink) are excluded from the core. Based on the four-momenta of infinitesimal string segments,

$$\delta p = \left\{ \frac{\partial X(\alpha, \beta)}{\partial \beta} \delta\alpha + \frac{\partial X(\alpha, \beta)}{\partial \alpha} \delta\beta \right\}, \tag{2}$$

with g being a Gaussian smoothing kernel, one computes the energy-momentum tensor and conserved currents for the core. The corresponding energy density $\varepsilon(\tau_0, \vec{x})$ and the flow velocity $\vec{v}(\tau_0, \vec{x})$ serve as initial conditions for the subsequent hydrodynamic evolutions. In case of corona, particle production occurs according to the usual string-breaking procedure, which has the advantage that in the low-density limit (for example for peripheral collisions) one recovers the conventional string model.

In Fig. 5, we show as an example the core energy density at $\tau_0 = 0.6$ fm/c for a high-multiplicity pp collision at 900 GeV, where high multiplicity here refers to a plateau height $dn/d\eta$ of 12.9, which is more than 3 times the average. We see a maximum energy density of about 50 GeV/fm^3, which indeed corresponds to the energy densities observed in central gold-gold collisions at 200 GeV. Even more, comparing with the spiky single-event results for gold-gold in Ref. [8], our pp distribution corresponds to one (of many) spikes in gold-gold at 200 GeV, which means a hydrodynamic treatment for pp is as good (or bad) as for gold-gold at 200 GeV.

B. Collective expansion

Having fixed the initial conditions, matter evolves according to the equations of ideal hydrodynamics, namely, the local

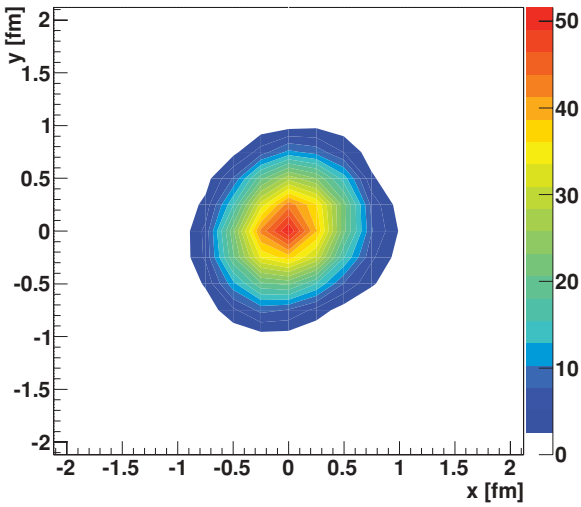

FIG. 5. (Color online) Initial energy density in GeV/fm^3 in a high-multiplicity pp collision ($dn/d\eta = 12.9$) at 900 GeV, at a space-time rapidity $\eta_s = 0$.

energy-momentum conservation,

$$\partial_\mu T^{\mu\nu} = 0, \quad T^{\mu\nu} = (\epsilon + p)u^\mu u^\nu - pg^{\mu\nu}, \tag{3}$$

and the conservation of net charges,

$$\partial N_k^\mu = 0, \quad N_k^\mu = n_k u^\mu, \tag{4}$$

with $k = B, S, Q$, where B, S, and Q refer to, respectively, baryon number, strangeness, and electric charge, and with u being the four velocity of the local rest frame. Solving the equations, as discussed in the appendix of Ref. [8], provides the evolution of the space-time dependence of the macroscopic quantities energy density $\varepsilon(x)$, collective flow velocity $\vec{v}(x)$, and the net flavor densities $n_k(x)$. Here, the crucial ingredient is the equation of state, which closes the set of equations by providing the ε dependence of the pressure p. As discussed in Ref. [8], we use an equation of state compatible with lattice gauge simulations (see Fig. 6).

Starting from the flux-tube initial condition, the system expands very rapidly. It hadronizes in the cross-over region,

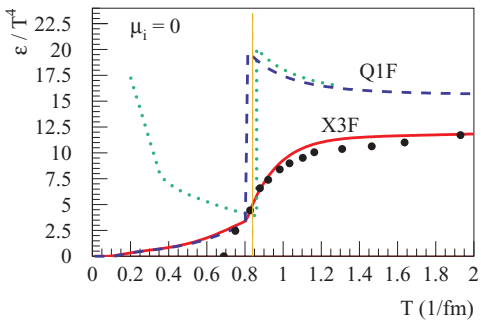

FIG. 6. (Color online) Energy density versus temperature, for our equation-of-state X3F (solid line), compared to lattice data [24] (points), and some other EoS choices (see Ref. [8]). The thin vertical line indicates the "hadronization temperature" T_H, that is, end of the thermal phase, when "matter" is transformed into hadrons.

where here "hadronization" is meant to be the end of the completely thermal phase: Matter is transformed into hadrons. We stop the hydrodynamical evolution at this point, but particles are not yet free. Our favorite hadronization temperature is 166 MeV, shown as the thin vertical line in Fig. 6, which is indeed right in the transition region, where the energy density varies strongly with temperature. At this point we employ statistical hadronization, which should be understood as hadronization of the quark-gluon plasma state into a hadronic system, at an early stage, not the decay of a resonance gas in equilibrium.

After this hadronization—although no longer thermal—the system still interacts via hadronic scatterings. The particles at their hadronization positions (on the corresponding hypersurface) are fed into the hadronic cascade model UrQMD [25,26], performing hadronic interactions until the system is so dilute that no interactions occur anymore. The "final" freeze-out position of the particles is the last interaction point of the cascade process, or the hydro hadronization position, if no hadronic interactions occurs.

In Fig. 7, we show the hydrodynamic evolution of the event corresponding to the initial energy density of Fig. 5, which can be considered as a typical example, with similar observations being true for randomly chosen events of this multiplicity ($dn/d\eta = 12.9$). We see that the system evolves immediately also transversely; the energy density drops very quickly. A very large transverse flow develops, typically around 70% of the velocity of light. This will have measurable consequences.

IV. ELEMENTARY DISTRIBUTIONS

We first check some elementary distributions. We use the EPOS 2.05 version, which has been optimized for heavy-ion scattering at RHIC, the same one as used in Ref. [8]. We could certainly improve the results by doing some "tuning" taking into account the new LHC results, but the purpose of this paper is more to show what we get from a straight application of the "heavy-ion model," here applied to pp at LHC. We only consider 900 GeV, for higher energies some reconsideration of our screening procedures will be necessary (work in progress). As usual, we work with the event-by-event mode, and hydrodynamics is only employed for high-density areas (core-corona separation).

In the following we compare three different scenarios:

(i) *full*: the full calculations, including hydro evolution and hadronic cascade;
(ii) *no casc*: calculation without hadronic cascade;
(iii) *no hydro*: calculation without hydro and without cascade.

We compare the corresponding calculations with experimental data, for pp scattering at 900 GeV.

In Fig. 8, we show pseudorapidity distributions of charged particles, compared to data from CMS [27] and ALICE [28,29]. The three scenarios do not differ very much and agree roughly with the data.

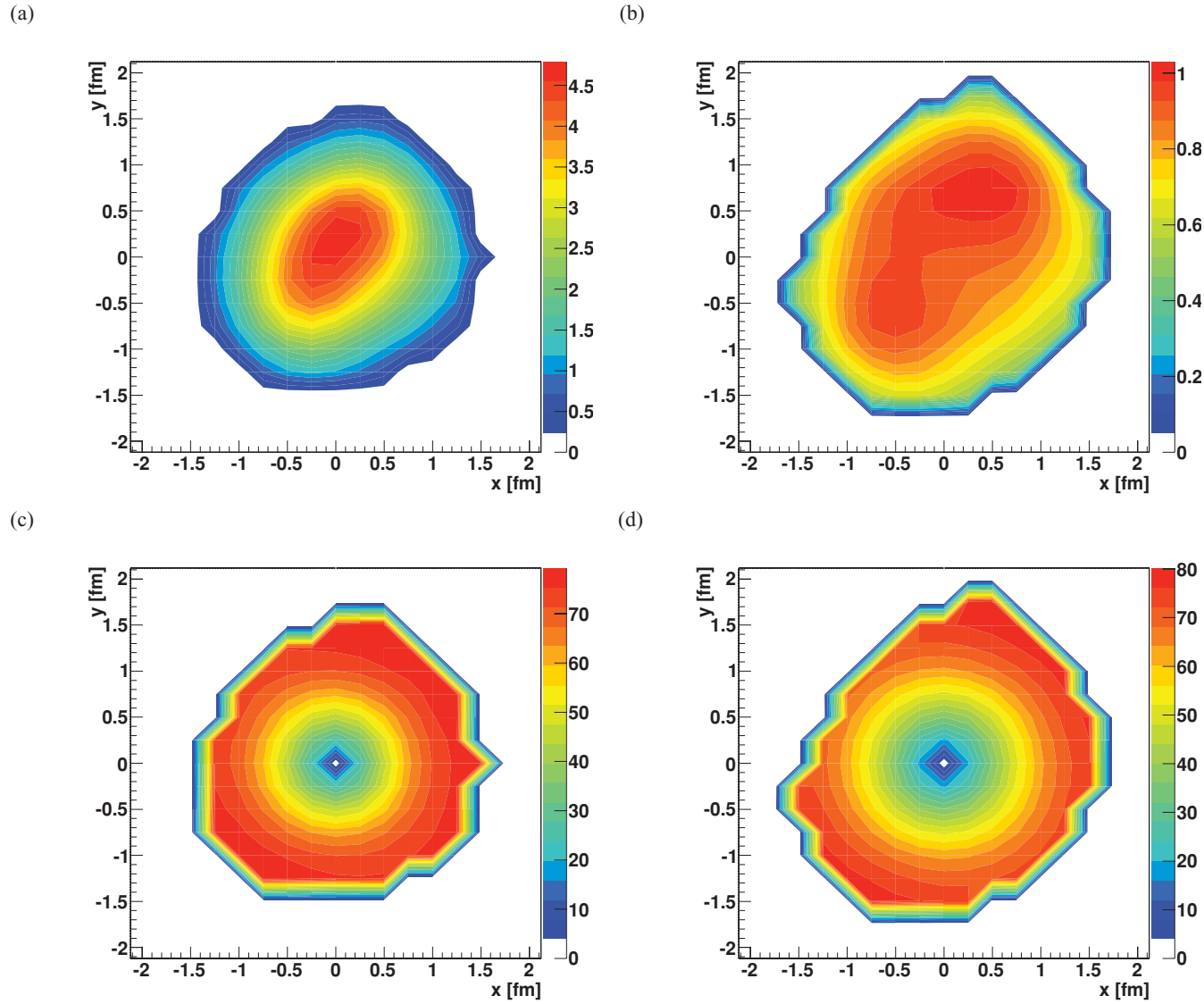

FIG. 7. (Color online) Energy density in GeV/fm^3 (top panels) and radial flow velocity in % relative to the velocity of light (bottom panels) for a high multiplicity pp collision ($dn/d\eta = 12.9$) at 900 GeV, at proper times $\tau = 1.3$ fm/c (left panels) and $\tau = 1.9$ fm/c (right panels), at a space-time rapidity $\eta_s = 0$.

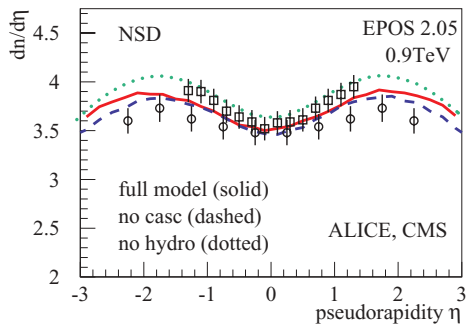

FIG. 8. (Color online) Pseudorapidity distributions in pp scattering at 900 GeV, compared to data (points). We show the full calculation (solid line), a calculation without hadronic cascade (dashed), and a calculation without hydro and without cascade (dotted).

We then investigate transverse momentum distributions. For minimum bias events, there is again little difference for the three scenarios (all of them reproduce the data within 20%), as seen in the top panel of Fig. 9. The situation changes drastically, when we consider high-multiplicity events, see the bottom panel of Fig. 9. Here the "no hydro" calculation underestimates the data by a factor of three, whereas the full calculation gets close to the data. This is a very typical behavior of collective flow: The distributions get harder at intermediate values of p_t (around 1–4 GeV/c).

In Fig. 10, we plot the mean transverse momentum as a function of the charged multiplicity, compared to data from ALICE [29]. The increase of the mean p_t with multiplicity is in our approach related to collective flow: With increasing multiplicity one gets higher initial energy densities, and more collective flow can develop. The data are therefore compatible with our flow picture, but other explanations are possible

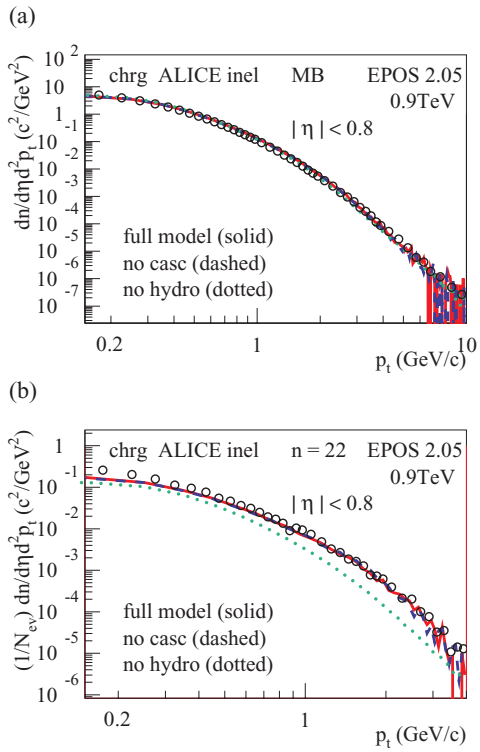

FIG. 9. (Color online) Transverse momentum distributions in pp scattering at 900 GeV, for minimum bias events (a) and high muliplicity events, $n = 22$ (b), compared to data (points).We show the full calculations (solid lines), a calculation without hadronic cascade (dashed), and a calculation without hydro and without cascade (dotted).

[30]—for a real proof one needs at least in addition the mean p_t behavior of heavier particles (protons, λ's, or even heavier), because the effect gets bigger with increasing mass.

V. BOSE-EINSTEIN CORRELATIONS IN HIGH MULTIPLICITY EVENTS

The space-time evolution of the full hydrodynamic approach will be completely different compared to the no hydro approach, where particles are directly produced from breaking

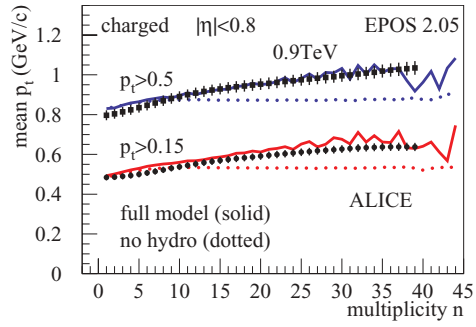

FIG. 10. (Color online) Mean transverse momentum as a function of the charged multiplicity in pp scattering at 900 GeV, compared to data (points). We show the full calculation (solid line), and a calculation without hydro and without cascade (dotted).

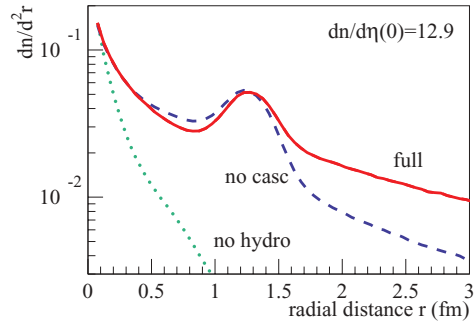

FIG. 11. (Color online) The distribution of formation points of π^+ as a function of the radial distance in high multiplicity events from pp scattering at 900 GeV, for the following scenarios: the full calculation (solid line), a calculation without hadronic cascade (dashed), and a calculation without hydro and without cascade (dotted).

strings, as can be seen from Fig. 11, where we plot the distribution of formation points of π^+ as a function of the radial distance:

$$r = \sqrt{x^2 + y^2} \tag{5}$$

[in the pp center of mass system (cms)]. Only particles with space-time rapidities around zero are considered. We compare again the three scenarios full (full calculation—flux-tube initial conditions, hydro, hadronic cascade), no casc (without hadronic cascade, only flux-tube initial conditions and hydro, hadronization as usual at 166 MeV), and no hydro (without hydro and without cascade, just flux-tube approach with string decay).

All calculations in this section refer to high-multiplicity events in pp scattering at 900 GeV, with a mean $dn/d\eta(0)$ equal to 12.9. The no hydro calculation (dotted line) gives as expected a steeply falling distribution as a function of r. In the two cases involving a hydrodynamical evolution, particle production is significantly delayed, even more in the case of the full calculation, with hadronic cascade. The bump in the two latter scenarios is attributable to particles being produced from the fluid; the small p_t contribution is attributable to corona particles.

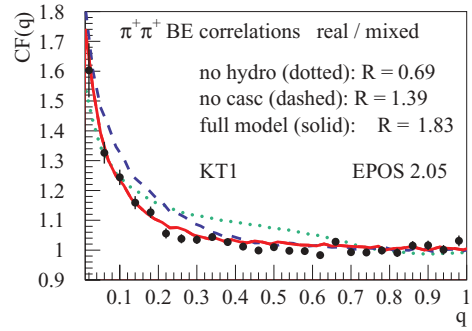

FIG. 12. (Color online) The correlation functions CF for π^+-π^+ pairs as obtained from our simulations, for the three different scenarios, for k_T bin KT1, compared to data (points).

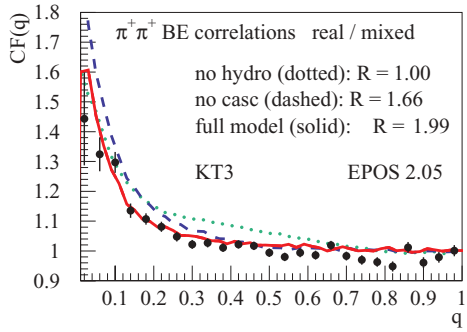

FIG. 13. (Color online) Same as Fig. 12, but for k_T range KT3.

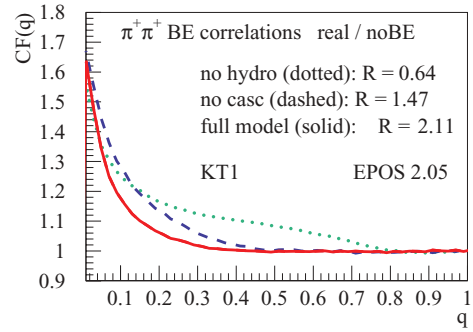

FIG. 15. (Color online) Same as Fig. 12, but for normalization via a simulation without BE correlation ("bare").

This particular space-time behavior of the hydrodynamic expansions should clearly affect Bose-Einstein correlations—which we investigate in the following. There is a long history of so-called femtoscopic methods [31–35], where the study of two-particle correlations provides information about the source function $S(\mathbf{P}, \mathbf{r}')$, being the probability of emitting a pair with total momentum $\mathbf{P}$ and relative distance $\mathbf{r}'$. Under certain assumptions, the source function is related to the measurable two-particle correlation function $\mathrm{CF}(\mathbf{P}, \mathbf{q})$ as

$$\mathrm{CF}(\mathbf{P}, \mathbf{q}) = \int d^3r' S(\mathbf{P}, \mathbf{r}') \left|\Psi(\mathbf{q}', \mathbf{r}')\right|^2, \qquad (6)$$

with $\mathbf{q}$ being the relative momentum, and where Ψ is the outgoing two-particle wave function, with $\mathbf{q}'$ and $\mathbf{r}'$ being relative momentum and distance in the pair center-of-mass system. The source function S can be obtained from our simulations, concerning the pair wave function, we follow Ref. [36], some details are given in [8]. -

Here, we investigate π^+-π^+ correlations. We evaluate Eq. (6), with Bose-Einstein (BE) quantum statistics included, but no Coulomb corrections. Weak decays are not carried out. In Figs. 12, 13 and 14, we show the results for different k_T intervals defined as (in MeV): KT1 = [100, 250], KT3 = [400, 550], and KT5 = [700, 1000], where k_T of the pair is defined as

$$k_T = \tfrac{1}{2}(|\vec{p}_t(\mathrm{pion1}) + \vec{p}_t(\mathrm{pion2})|). \qquad (7)$$

We compare the three different scenarios: full calculation (solid line), calculation without hadronic cascade (dashed), and calculation without hydro and without cascade (dotted),

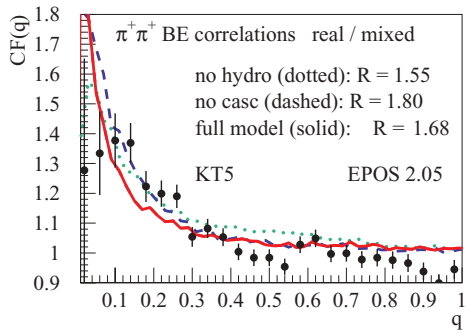

FIG. 14. (Color online) Same as Fig. 12, but for k_T range KT5.

and data from ALICE [37]. The data are actually not Coulomb corrected, because the effect is estimated to be small compared to the statistical errors. We consider here the high multiplicity class, with $dn/d\eta(0) = 11.2$, close to the value of 12.9 from our simulated high-multiplicity events. We compare with the real data (not polluted with simulations), normalized via mixed events, and we do the same with our simulations. Despite the limited statistics, in particular at large k_T, we see very clearly that the "full" scenario, including hydro evolution and hadronic cascade, seems to fit the data much better then the two other ones. Usually people like to extract radii from these distributions, so when we make a fit of the form

$$\mathrm{CF} - 1 = \lambda \exp(-R|\mathbf{q}|), \qquad (8)$$

in the $|\mathbf{q}|$ range from 0.05 to 0.70. We obtain the radii given in the figure. So the radii are very different, varying from 0.69 fm (no hydro approach) to 1.80 fm (full model), which is understandable from Fig. 11. We prefer an exponential fit rather than a Gaussian, simply because the former one works; the latter one does not. We do not want to give a precise meaning to R; it simply characterizes the distribution.

Normalizing by mixed events is something one can easily do experimentally (this is why we compare with these data), but it is clear that one has still unwanted correlations, such as those owing to energy-momentum conservation, which is not an issue in mixed events. Doing simulations, life is easier. We can take simulations without BE correlations as base line,

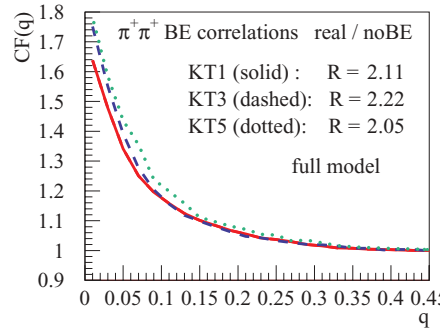

FIG. 16. (Color online) Correlation function, normalized by using a simulation without BE correlation ("bare"), for three k_T intervals.

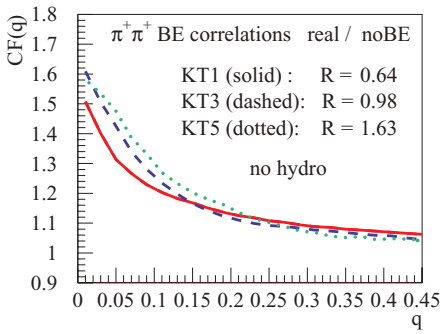

FIG. 17. (Color online) As Fig. 16, but calculation without hydro and without cascade.

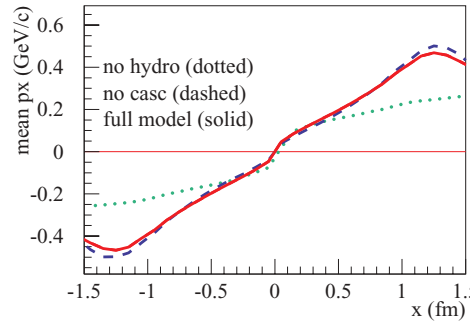

FIG. 19. (Color online) Momentum-space correlation for the different scenarios.

rather than mixed events. This is referred to as "real/bare" normalization (to be distinguished from the "real/mixed" case discussed earlier). The corresponding results are shown in Fig. 15, the solid line (full calculation) is now completely horizontal away from the peak region; the radius from the exponential fit is 2.10 fm instead of 1.80 fm for the "mixed" normalization. For the other k_T regions, the situation is similar; the final results for all three k_T regions for the full calculation is shown in Fig. 16, together with the the radii from the exponential fit: They are almost identical, around 2 fm.

We get to the same conclusion as outlined in Ref. [37]: The radii are k_T independent, contrary to what has been observed in AuAu scattering.

How can it be that our hydrodynamic scenario gives a strong k_T dependence in AuAu, but not in pp? To answer this question, we compute the "true" correlation function (real/bare normalization) for the calculation without hydro and without cascade (just string decay). The results are shown in Fig. 17. Surprisingly, here we get a strong k_T dependence of the radii, but the "wrong" way: We have 0.64 fm for KT1 and 1.63 fm for KT5. Actually, such a behavior is quite normal, as seen from Fig. 18: The distribution is broader for high p_t particles, because high p_t resonances live longer and can move further out before decaying. This effect is, in principle, also present in AuAu scattering, but it is much more visible for the small pp system. So in pp we have two competing effects:

(i) radii increase with k_T, owing to the bigger size of the source of the high p_t particles compared to the low p_t ones;
(ii) radii decrease with k_T, as in AuAu (see Ref. [8]), in case collective flow, owing to the p-x correlation.

As seen in Fig. 19, this p-x correlation exists indeed for the case of hydrodynamic evolutions and is much smaller in the basic scenario.

So in the hydro scenarios, the two competing effects roughly cancel, the radii are k_T independent. To really see the x-p correlation, one needs to "divide out" the trivial k_T dependence owing to the p_t dependence of the single-particle source sizes, which we do by considering the k_T dependence of $R/R_{\rm bas}$, with the reference radius $R_{\rm bas}$ referring to the no hydro scenario (without hydro, without cascade) (see Fig. 20): The ratio $R/R_{\rm bas}$ decreases with k_T as a manifestation of the x-p correlation, as a consequence of the hydrodynamic expansion.

An alternative way of getting out unwanted correlations would be the consideration of double ratios such as

$$\frac{\text{CF(full scenario with BE)/CF(full scenario w/o BE)}}{\text{CF(no hydro scen with BE)/CF(no hydro scen w/o BE)}}, \tag{9}$$

where basic scenario refers to the calculation without hydro and without hadronic cascade.

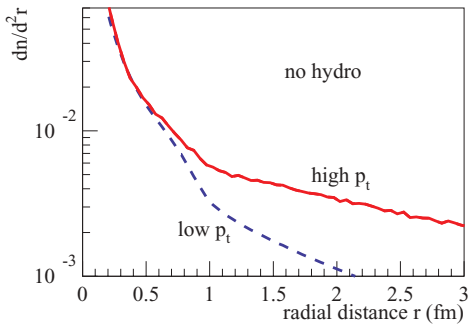

FIG. 18. (Color online) The distribution of formation points of particles as a function of the radial distance, for the scenario "without hydro and without cascade" for high p_t and low p_t particles.

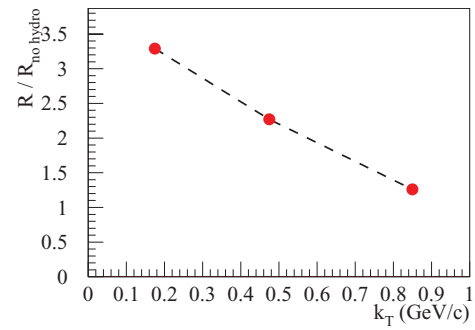

FIG. 20. (Color online) The k_T dependence of $R/R_{\rm bas}$. The ratio decreases significantly with k_T, a clear "flow signal."

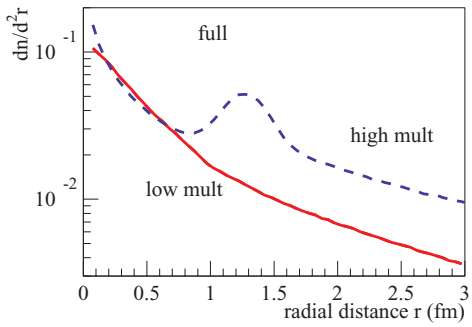

FIG. 21. (Color online) The distribution of formation points of π^+ as a function of the radial distance in pp scattering at 900 GeV, for the full calculation. We compare the results for high-multiplicity events (dashed line) with the result for low-multiplicity events (solid line).

VI. BOSE-EINSTEIN CORRELATIONS IN LOW MULTIPLICITY EVENTS

For completeness, we discuss in the following low multiplicity events, with the mean $dn/d\eta(0$ being equal to 2.7, comparable to the low multiplicity bin in the ALICE publication [37].

In Fig. 21, we plot the distribution of formation points of π^+ as a function of the radial distance, for low-multiplicity events, compared to the results shown earlier for high-multiplicity ones. In the former case, there is no "hydro bump" any more, owing to the fact that the number of particles coming from the hydro phase is small; most particles are attributable to simple string decay. We recall that also in pp the core-corona procedure is very important: Only regions with strongly overlapping strings contribute to the core (and are treated via hydrodynamics),and this overlap is more likely to happen in high-multiplicity events.

As a consequence of the reduced hydro contribution, the difference between the full calculation and the no hydro version is relatively small in low-multiplicity events, as can be seen from Fig. 22, where we show the correlation functions for the different k_T intervals, comparing the two scenarios full model (solid line) and no hydro (dotted lines), together with the experimental data from Ref. [37]. The radii R for the exponential fits of the full model are 1.56 (KT1), 1.38 (KT3), and 1.51 (KT5), to be compared with the experimental value of 1.44 (k_T integrated). Both scenarios, full model and no hydro, fit the experimental correlation functions equally well. This means also that our full aproach (hydro based on flux tube initial conditions) successfully describes the data, for high- and low-multiplicty events, although the relative importance of the hydro contribution is very different for high- and low-multiplicity events.

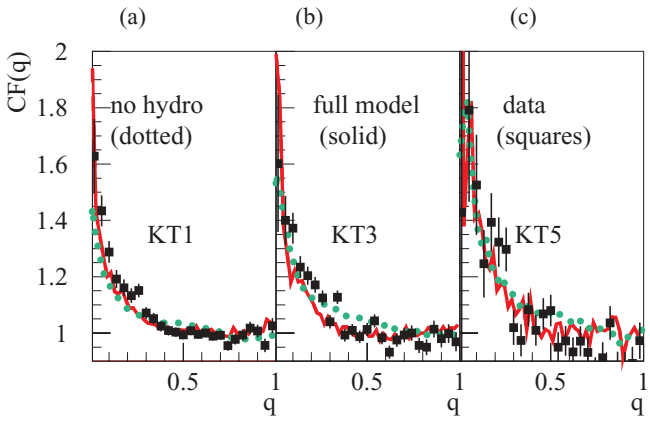

FIG. 22. (Color online) The correlation functions CF for π^+-π^+ pairs for low-multiplicity events. As in the data, we normalize via mixed events.

VII. SUMMARY

After having introduced recently a sophisticated approach of hydrodynamic expansion based on flux-tube initial conditions for AuAu collisions at RHIC, we now employ exactly the same picture to pp scattering at 900 GeV, which is in particular justified for high multiplicity events. A very interesting application are BE correlations. We have shown that as in heavy-ion scattering the hydrodynamic expansion leads to momentum-space correlations, which clearly affect the correlation functions. To see the signal is nontrivial owing to the fact that in addition to the x-p correlations (which leads to decreasing radii with k_T, there is a second effect which works the other way around: The single-particle source size is p_t dependent, which is an important effect in pp; not so in heavy-ion scattering. In this sense we can interpret the k_T independence of the radii as a real flow effect. Our simulation does not only reproduce the k_T independence, but also the whole correlation functions, which is not at all reproduced from the no hydro scenario without hydro and without cascade. So the correlation data provide a very strong evidence for a collective hydrodynamic expansion in pp scattering at the LHC.

ACKNOWLEDGMENTS

This research has been carried out within the scope of the ERG (GDRE) "Heavy ions at ultra-relativistic energies," a European Research Group comprising IN2P3/CNRS, Ecole des Mines de Nantes, Universite de Nantes, Warsaw University of Technology, JINR Dubna, ITEP Moscow, and Bogolyubov Institute for Theoretical Physics NAS of Ukraine. Iu. K. acknowledges partial support by the MESU of Ukraine and Fundamental Research State Fund of Ukraine, Agreement No. F33/461-2009. Iu. K. and K. W. acknowledge partial support by Ukrainian-French Grant No. "DNIPRO," Agreement No. M/4-2009 with MESU of Ukraine. T.P. and K.W. acknowledge partial support by a PICS (CNRS) with KIT (Karlsruhe). K.M. acknowledges partial support by RFBR-CNRS Grants No. 08-02-92496-NTsNIL_a and No. 10-02-93111-NTsNIL_a.

[1] P. Huovinen, P. F. Kolb, U. W. Heinz, P. V. Ruuskanen, and S. A. Voloshin, Phys. Lett. B **503**, 58 (2001).
[2] T. Hirano and K. Tsuda, Phys. Rev. C **66**, 054905T (2002).
[3] S. A. Bass and A. Dumitru, Phys. Rev. C **61**, 064909 (2000).
[4] D. Teaney, J. Lauret, and E. V. Shuryak, Phys. Rev. Lett. **86**, 4783 (2001).
[5] T. Hirano, U. W. Heinz, D. Kharzeev, R. Lacey, and Y. Nara, Phys. Lett. B **636**, 299 (2006).
[6] C. Nonaka and S. A. Bass, Nucl. Phys. A **774**, 873 (2006); Phys. Rev. C **75**, 014902 (2007).
[7] R. P. G. Andrade, F. Grassi, Y. Hama, T. Kodama, W. L. Qian, Phys. Rev. Lett. **101**, 112301 (2008).
[8] K. Werner, Iu. Karpenko, T. Pierog, M. Bleicher, K. Mikhailov, Phys. Rev. C **82**, 044904 (2010).
[9] L. D. Landau, Izv. Akad. Nauk SSSR **17**, 51 (1953).
[10] P. Carruthers, Ann. N.Y. Acad. Sci. **229**, 91 (1974).
[11] M. Luzum and P. Romatschke, Phys. Rev. Lett. **103**, 262302 (2009).
[12] S. Prasad *et al.*, Phys. Rev. C **82**, 024909 (2010); G. Orta *et al.*, Acta Phys. Pol. **B41**, 837 (2010).
[13] B. Andersson, G. Gustafson, G. Ingelman, and T. Sjostrand, Phys. Rept. **97**, 311983.
[14] K. Werner, Phys. Rep. **232**, 871993.
[15] H. J. Drescher, M. Hladik, S. Ostapchenko, T. Pierog, and K. Werner, Phys. Rept. **350**, 932001.
[16] A. Capella, U. Sukhatme, C. I. Tan, and J. Tran Thanh Van, Phys. Rept. **236**, 2251994.
[17] L. D. McLerran and R. Venugopalan, Phys. Rev. D **49**, 2233 (1994); **49**, 3352 (1994); **50**, 2225 (1994).
[18] Yu. V. Kovchegov, Phys. Rev. D **54**, 5463 (1996).
[19] E. Iancu and R. Venugopalan, *Quark Gluon Plasma*, edited by R. C. Hwa and X. N. Wang (World Scientific, Singapore, 2004).
[20] A. Kovner, L. D. McLerran, and H. Weigert, Phys. Rev. D **52**, 3809 (1995); **52**, 6231 (1995).
[21] F. Gelis, E. Iancu, J. Jalilian-Marian, and R. Venugopalan, arXiv:1002.0333.
[22] K. Werner, and F.-M. Liu, T. Pierog, Phys. Rev. C **74**, 044902 (2006)
[23] K. Werner, Phys. Rev. Lett. **98**, 152301 (2007).
[24] Y. Aoki, Z. Fodor, S. D. Katz, K. K. Szabo, J. High Energy Phys. **0601**, 89 (2006).
[25] M. Bleicher *et al.*, J. Phys. G **25**, 1859 (1999).
[26] H. Petersen, J. Steinheimer, G. Burau, M. Bleicher, and H. Stocker, Phys. Rev. C **78**, 044901 (2008).
[27] CMS. Collaboration, J. High Energy Phys. **02** (2010) 041.
[28] ALICE collaboration, arXiv:1007.0719.
[29] K. Aamodt *et al.*, ALICE. collaboration, Eur. Phys. J. C **68**, 89 (2010).
[30] L. McLerran, M. Praszalowicz, Acta Physica Polon. B **41**, 1917 (2010).
[31] G. I. Kopylov and M. I. Podgoretsky, Sov. J. Nucl. Phys. **15**, 219 (1972).
[32] G. I. Kopylov and M. I. Podgoretsky, Sov. J. Nucl. Phys. **18**, 336 (1974).
[33] S. Pratt, Phys. Rev. Lett. **53**, 1219(1984).
[34] M. A. Lisa, Scott Pratt, Ron Soltz, Urs Wiedemann, Ann. Rev. Nucl. Part. Sci. **55**, 357 (2005).
[35] A. Kisiel, W. Florkowski, and W. Broniowski, Phys. Rev. C **73**, 064902 (2006).
[36] R. Lednicky, Phys. Part. Nuclei **40**, 307 (2009).
[37] ALICE collaboration, arXiv:1007.0516.